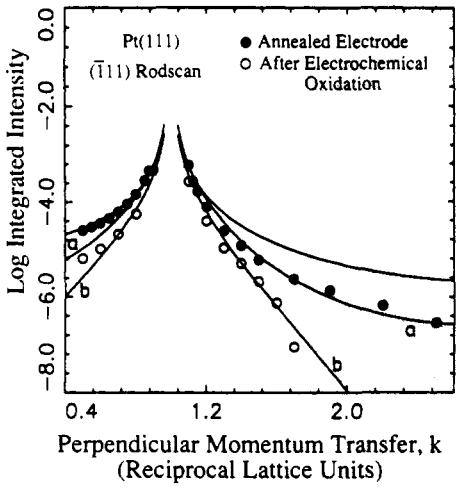

Figure 5. Ideal CTR profile and fits to experimental data (●, annealed electrode; ○, after electrochemical oxidation) employing contributions from both types of roughening.

surface, there were also some discrepancies. However, it is also clear that the fit was greatly improved over that for the model where the only contribution to the roughness arose from displaced atoms still occupying lattice positions. Especially notable was the fact that, in this case, the downward curvature in the data was reproduced (Figure 4c).

Finally, we attempted fits to the data using a weighted combination of both models of roughness, and the rsults are presented in Figure 5. For the annealed surface the roughness can be described as being due entirely to displaced atoms occupying lattice positions. From the fits to the data, we obtain a value for the roughness of 3.3 ± 0.3 Å. On the other hand, for the electrochemically oxidized electrode we find significant contributions from both types of roughness. From the fits to the data we obtain values of 3.35 ± 0.34 and 2.05 ± 0.35 Å for roughness due to displaced atoms occupying lattice positions and randomly displaced atoms, respectively.

These measurements suggest that although the surface, as prepared, has some roughness, it is essentially due to displaced atoms occupying lattice positions so that the surface is relatively well ordered. Exposure of the electrode to an electrolyte solution and the application of the rest potential did not affect the interfacial structure. Similarly, the reductive desorption of the iodine adlayer (at −1.0 V) did not alter the surface structure.

On the other hand, the effects of applying a potential of +1.0 V for 15 min were dramatic. The surface becomes significantly rougher, and in addition, there is a significant degree of roughness due to randomly displaced atoms. It is interesting to note, however, that the roughness due to displaced atoms occupying lattice positions was not significantly changed. This suggests that as the outermost layers of the surface are amorphized by the electrochemical treatment, atoms from the region proximal to the surface are displaced so as to maintain essentially the same degree of fractional occupancy in these layers. This might suggest a roughening mechanism where as the outermost layers amorphize, the subsequent layers largely retain the structural features of the original surface. Thus, the net effect of the electrochemical roughening is to, in essence, cover the surface with a largely amorphous layer of Pt atoms.

We are continuing our studies on the use of the CTR technique to study electrochemically induced roughening in the presence of other strongly chemisorbed species.

Conclusions

We have demonstrated the applicability of the CTR technique to study electrochemically induced roughening of an iodine-pretreated Pt(111) electrode. We find that the annealed surface is best described as one where surface atoms have been displaced but still occupy lattice positions whereas electrooxidative roughening gives rise to a largely amorphous surface layer.

Acknowledgment. This work was carried out in collaboration with Dr. B. Ocko at Brookhaven National Laboratory whose help is greatly appreciated. Our work was generously funded by the Office of Naval Research, the Army Research Office, and the National Science Foundation. H.D.A. acknowledges support by the Presidential Young Investigator program at NSF and the A. P. Sloan Foundation. D.A. acknowledges support by the MARC Fellowship Program at NIH. NSLS is supported by the Department of Energy.

The Local Structure of $Bi_{2.2}Sr_{1.8}Cu_{1-x}Fe_xO_y$ Single Crystals Determined by Scanning Tunneling Microscopy

Chunming Niu and Charles M. Lieber*

Department of Chemistry and Division of Applied Sciences, Harvard University, Cambridge, Massachusetts 02138 *(Received: October 7, 1991; In Final Form: November 26, 1991)*

Scanning tunneling microscopy (STM) has been used to characterize the surface structure of cleaved single crystals of $Bi_{2.2}Sr_{1.8}CuO_y$ and $Bi_{2.2}Sr_{1.8}Cu_{0.9}Fe_{0.1}O_y$. Images of $Bi_{2.2}Sr_{1.8}CuO_y$ exhibit a one-dimensional superstructure with a modulation period of 25.1 ± 0.3 Å. The atomic structure in these images is ordered and shows no evidence of local distortions due to Sr^{2+} substitution and/or extra oxygen in the BiO layer. Substitution of Fe in the CuO layer of this material caused substantial changes in the superstructure and the BiO layer atomic structure. The superstructure period in $Bi_{2.2}Sr_{1.8}Cu_{0.9}Fe_{0.1}O_y$ determined from the analysis of STM images and two-dimensional Fourier transform power spectra, 22.8 ± 1.0 Å, was smaller and less regular than that observed for $Bi_{2.2}Sr_{1.8}CuO_y$ samples. In addition, the atomic structure of the Fe-substituted material exhibited significant disorder. These results are discussed in terms of lattice mismatch and bonding between the BiO and the Cu(Fe)O layers of this material.

Introduction

The bismuth-based copper oxide superconductors, $Bi_2Sr_2Ca_{n-1}Cu_nO_{2n+4}$ (n = 1-3), comprise a structurally and chemically rich class of materials that exhibit a wide range of superconducting properties (Figure 1).[1,2] One unique feature of these bismuth-based materials that distinguishes them from other copper oxide superconductors is a strong, one-dimensional

* Author to whom correspondence should be addressed.

(1) Michel, C.; Hervieu, M.; Borel, M. M.; Crandin, A.; Deslandes, F.; Provost, J.; Raveau, B. *Z. Phys.* **1987**, *B68*, 421.
(2) Maeda, H.; Tanaka, Y.; Fukutomi, M.; Asano, T. *Jpn. J. Appl. Phys.* **1988**, *27*, L209.

0022-3654/92/2096-3419$03.00/0

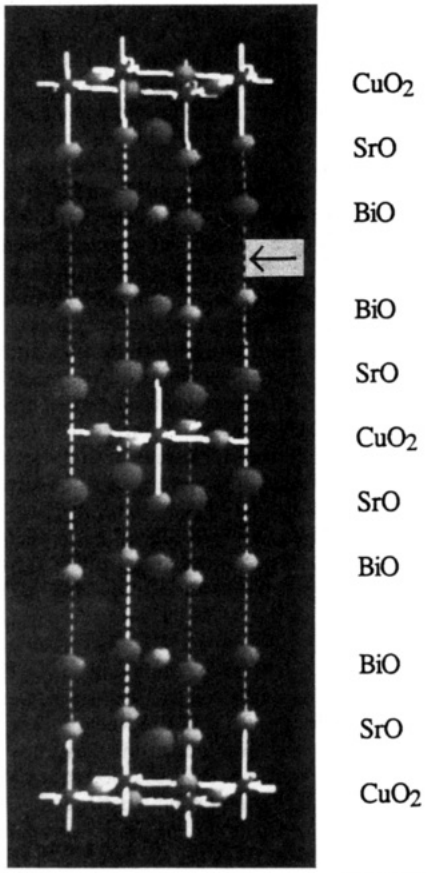

Figure 1. Model structure of the $n = 1$ compound $Bi_2Sr_2CuO_6$. The c axis is oriented vertical with respect to the page. The arrow indicates the preferential cleavage plane between the weakly interacting (separation = 3.1–3.3 Å) BiO/BiO double layers.

structural modulation.[3,4] Early diffraction studies showed that this modulation involves displacements of the Bi, Sr, and Cu metal atoms from their ideal positions in the crystal lattice;[5] however, the underlying origin of this modulation and the precise oxygen displacements associated with the superstructure remain ambiguous. Resolution of the key details of this structural modulation have been hampered in part by the incommensurate nature of the superstructure. Recent diffraction studies employing four-dimensional superspace groups have led to an improved refinement of the modulated structure in $Bi_2Sr_2CaCu_2O_8$, although the positions of the atomic sites in the BiO layer remain somewhat uncertain.[6-8] The difficulties associated with characterizing the microscopic structure in these materials are further exacerbated for metal-doped systems since metal substitution can occur at different sites (with varying degrees of site selectivity) and can change the oxygen content.

An alternative approach that has been used to address the structure and electronic properties of the BiO layer in $Bi_2Sr_2CaCu_2O_8$ is scanning tunneling microscopy (STM).[9-15] STM is ideally suited to characterize the modulation for several reasons. First, the high resolution of STM is not degraded by incommensurate superstructures and disorder since it is a real-space technique. In addition, it is well-established that crystals of $Bi_2Sr_2Ca_{n-1}Cu_nO_{2n+4}$ cleave preferentially between the weakly interacting BiO/BiO double layers (Figure 1) to expose a BiO surface layer that is structurally and compositionally similar to the bulk.[9,11,12,16] For example, the *average* BiO surface structure determined by STM and low-energy electron diffraction and the BiO layer structure determined from bulk measurements are the same. In addition, it is now established that the surface and bulk superconducting properties determined by photoemission[16] and infrared[17] spectroscopies, respectively, are similar. Thus, high-resolution surface experiments on these materials can provide information important to understanding their bulk properties.

To date, STM studies of the $n = 2$ system, $Bi_2Sr_2CaCu_2O_y$, have elucidated details of the atomic structure and electronic states of the BiO layer in this material.[9-15] Other questions, including the origin of the one-dimensional superstructure, remain unanswered. In this report we describe the first atomic resolution STM study of the $n = 1$ material, $Bi_2Sr_2CuO_y$. This compound is particularly attractive for continued investigations since (1) the structure is less complex than the $n = 2$ or $n = 3$ materials,[18-22] (2) small changes in the Bi:Sr ratio affect a transition from an insulating to superconducting phase,[1,23,24] and (3) the electronic states near the Fermi level have been proposed to differ from the $n = 2$ material.[25] Hence, it is expected that STM studies of $Bi_2Sr_2CuO_y$ could provide new insight into the incommensurate modulation in the $Bi_2Sr_2Ca_{n-1}Cu_nO_{2n+4}$ system and also serve as an important comparison with previous studies of the $n = 2$ material.

Experimental Methods

Single crystals of $Bi_2Sr_2Cu_{1-x}Fe_xO_y$ ($0 \le x \le 0.1$) were grown from CuO-rich melts. Briefly, a homogeneous mixture of high-purity (>99.99%) Bi_2O_3, $SrCO_3$, CuO, and Fe_2O_3 powders were melted at 980 °C, cooled at 3 °C/h to 800 °C, and then furnace cooled to room temperature. Single crystals were removed mechanically from the solidified melt[12] and were subsequently annealed in oxygen at 450 °C for 1 week to relieve extrinsic strain in the lattice. X-ray diffraction measurements (001 lines) were used to select single-phase 2201 crystals. The stoichiometry of the metals in the single crystals was determined with an accuracy of 0.6% by inductively coupled plasma emission spectroscopy (ICPES). In addition, all samples were characterized by magnetic susceptibility and four-probe resistivity measurements prior to the

(3) Subramanian, M. A.; Torardi, C. C.; Calabrese, J. C.; Gopalakrishnan, J.; Morrisey, K. J.; Askew, T. R.; Flippen, R. B.; Chowdhry, U.; Sleight, A. W. *Science* **1988**, *239*, 1015.
(4) Yamamoto, A.; Onoda, M.; Takayama-Muromachi, E.; Izumi, F. *Phys. Rev. B* **1990**, *42*, 4228.
(5) Gao, Y.; Lee, P.; Coppens, P.; Subramanian, M. A.; Sleight, A. W. *Science* **1988**, *241*, 954.
(6) Petricek, V.; Coppens, P.; Becker, P. *Acta Crystallogr.* **1985**, *A41*, 478.
(7) Gao, Y.; Lee, P.; Graafsma, H.; Yeh, J.; Bush, P.; Petricek, V.; Coppens, P. *Chem. Mater.* **1990**, *2*, 323.
(8) Yamamoto, A.; Onoda, M.; Muromachi, E. T.; Izumi, F. *Phys. Rev. B* **1990**, *42*, 4228.
(9) Kirk, M. D.; Nogami, J.; Baski, A. A.; Mitzi, D. D.; Kapitulnik, A.; Geballe, T. H.; Quate, C. F. *Science* **1988**, *242*, 1673.
(10) Zhang, Z.; Wang, Y. L.; Wu, X. L.; Huang, J.-L.; Lieber, C. M. *Phys. Rev. B* **1990**, *42*, 1082.
(11) Shih, C. K.; Feenstra, R. M.; Kirtley, J. R.; Chandrashekhar, G. V. *Phys. Rev. B* **1989**, *40*, 2682.
(12) (a) Wu, X. L.; Zhang, Z.; Wang, Y. L.; Lieber, C. M. *Science*, **1990**, *248*, 1211. (b) Wu, X. L.; Wang, Y. L.; Zhang, Z.; Lieber, C. M. *Phys. Rev. B* **1991**, *43*, 8729.
(13) Tanaka, M.; Takahashi, T.; Katayama-Yoshida, H.; Yamazaki, S.; Fujinami, M.; Okaba, Y.; Mizutani, W.; Ono, M.; Kajimura, K. *Nature* **1989**, *339*, 691.
(14) Wang, C.; Giambattista, B.; Slough, C. G.; Coleman, R. V.; Subramanian, M. A. *Phys. Rev. B.* **1990**, *42*, 8890.
(15) Shih, C. K.; Feenstra, R. M.; Chandrashekhar, G. V. *Phys. Rev. B* **1991**, *43*, 7913.
(16) Wells, B. O.; Shen, Z.-X.; Dessau, D. S.; Spicer, W. E.; Olson, C. G.; Mitzi, D. B.; Kapitulnik, A.; List, R. S.; Arko, A. *Phys. Rev. Lett.* **1990**, *65*, 3056.
(17) Schlesinger, Z.; Collins, R. T.; Holtzberg, F.; Feild, C.; Koren, G.; Gupta, A.; *Phys. Rev. B* **1990**, *41*, 11237.
(18) Torardi, C. C.; Subramanian, M. A.; Calabrese, J. C.; Gopalakrishnan, J.; McCarron, E. M.; Morrissey, K. J.; Askew, T. R.; Flippen, R. B.; Chowdhry, U.; Sleight, A. W. *Phys. Rev. B* **1988**, *38*, 225.
(19) Torrance, J. B.; Tokura, Y.; LaPlaca, S. J.; Huang, T. C.; Savoy, R. J.; Nazzal, A. I. *Solid State Commun.* **1988**, *66*, 703.
(20) Onoda, M.; Sato, M. *Solid State Commun.* **1988**, *67*, 79.
(21) Roth, R. S.; Rawn, C. J.; Bendersky, L. A. *J. Mater. Res.* **1990**, *5*, 46.
(22) Matsui, Y.; Takekawa, S.; Horiuch, S. *Jpn. J. Appl. Phys.* **1988**, *27*, L1873.
(23) Sinclair, D. C.; Irvine, J. T. S.; West, A. R. *Jpn. J. Appl. Phys.* **1990**, *29*, L2002.
(24) Fleming, R. M.; Sunshine, S. A.; Schneemeyer, L. F.; Van Dover, R. B.; Cava, R. J.; March, P. M.; Waszczak, J. V.; Glarum, S. H.; Zahurak, S. M.; DiSalvo, F. J. *Physica C* **1991**, *173*, 37.
(25) Shen, Z. X.; Lindberg, P. A. P.; Soukiassian, P.; Eom, C. B.; Lindau, I.; Spicer, W. E.; Geballe, T. H. *Phys. Rev. B* **1989**, *39*, 823.

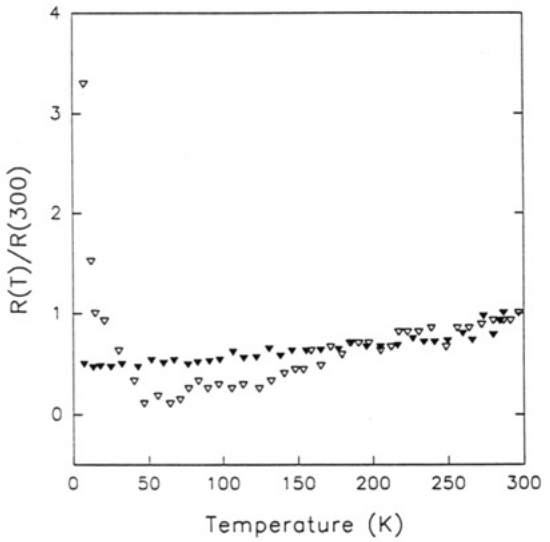

Figure 2. Plots of resistance versus temperature for $Bi_{2.2}Sr_{1.8}CuO_y$ (▼) and $Bi_{2.2}Sr_{1.8}Cu_{0.9}Fe_{0.1}O_y$ (▽) determined on single crystal samples.

STM experiments to ensure the quality of the single crystal materials.

The STM measurements were made with a modified commercial instrument (Nanoscope, Digital Instruments, Inc., Santa Barbara, CA) operated in an argon-filled glovebox equipped with a purification system that reduced the concentrations of H_2O and O_2 to ca. 1 ppm.[26] Reproducible and stable (>8 h) STM images of the BiO layer were obtained for samples cleaved in situ. Previously, STM studies of $Bi_2Sr_2CaCu_2O_8$ carried out in this glovebox and in ultrahigh vacuum have shown that the same BiO surface structure is observed under both conditions. It is thus apparent that the relatively inert BiO surface is not contaminated in the glovebox environment. Images were acquired in the constant-current mode using Pt–Ir alloy (80%–20%) tips that were mechanically sharpened in the glovebox. Other experimental details have been described elsewhere.[10,12]

Results

Bulk Analyses. ICPES studies of $x = 0$ and $x = 0.1$ crystals showed that the metal ion stoichiometry was $Bi_{2.2}Sr_{1.8}CuO_y$ and $Bi_{2.2}Sr_{1.8}Cu_{0.9}Fe_{0.1}O_y$, respectively. These results indicate that Fe substitutes primarily for Cu as expected on the basis of previous studies.[27] In addition, these data show that our crystals contain an excess of Bi and are deficient in Sr on the basis of the ideal 2201 formulation; however, the Bi/Sr deviation from the 2:2 stoichiometry is the same in both undoped and doped samples. X-ray diffraction patterns of the undoped and doped samples could be indexed using the orthorhombic cell of the 2201 phase.[27]

Representative resistance versus temperature curves obtained on single crystal $Bi_{2.2}Sr_{1.8}O_y$ and $Bi_{2.2}Sr_{1.8}Cu_{0.9}Fe_{0.1}O_y$ samples are shown in Figure 2. The pure material exhibits weak metallic behavior down to 5 K with no evidence for a superconducting transition. This result is in agreement with that reported by Fleming et al.[24] The oxygen-annealed $Bi_{2.2}Sr_{1.8}Cu_{0.9}Fe_{0.1}O_y$ also shows weak metallic behavior from 300 to 50 K but undergoes a metal–insulator transition at 50 K; i.e., the resistivity increases below 50 K. Notably, the bulk conductivity at room temperature where the STM measurements were made is metallic for both samples.

STM Investigations. The STM studies were carried out on undoped and doped single crystals that had been characterized as described above. Single crystals of these materials are well-known to cleave preferentially along the weakly interacting BiO/BiO double layers (Figure 1) to yield a BiO surface that is structurally and compositionally similar to the bulk.[9–15] A typical gray scale image of the BiO layer of a cleaved $Bi_{2.2}Sr_{1.8}CuO_y$ single crystal is shown in Figure 3. The image was acquired in the constant-current mode with a bias voltage of 145 mV. The tetragonal atomic lattice and one-dimensional superstructure are resolved simultaneously in Figure 3. The average lattice spacing of the atomic structure determined from several high-quality images is 3.8 ± 0.2 Å. This lattice spacing is consistent with the average Bi–Bi or O–O distances in the Bi–O layers determined by X-ray crystallography[4,5,27] and is similar to previous data obtained on $Bi_2Sr_2CaCu_2O_8$ crystals.

Figure 3 also exhibits a prominent one-dimensional superstructure along the *b* direction of the orthorhombic cell. We find that the superstructure modulation in the annealed $Bi_{2.2}Sr_{1.8}CuO_y$ crystals is more regular than reported previously in studies of $Bi_2Sr_2CaCu_2O_8$.[9–12] The average modulation period determined from several images is 25.1 ± 0.3 Å. This period, which is in agreement with the average modulation determined by diffraction,[20] is incommensurate with the underlying lattice. Despite the incommensurate nature of the superstructure, it is straight-

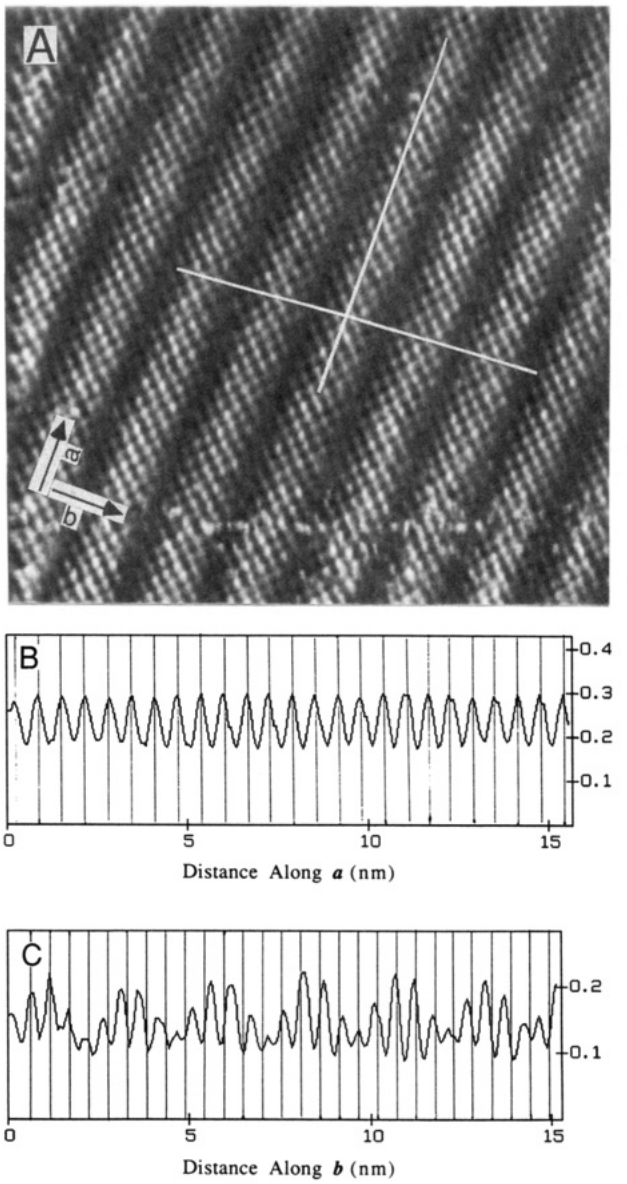

Figure 3. (A) 200 × 200 Å² gray scale STM image of $Bi_{2.2}Sr_{1.8}CuO_y$ recorded with a bias voltage of 145 mV and a tunneling current of 0.65 nA. The orthorhombic axes, *a* and *b*, are marked with arrows. (B, C) High-resolution cross sectional views along the *a* and *b* directions, respectively. The cross sections were taken along the white lines in the STM image (A). The lattice spacing is regular along *a* but exhibits compressive and expansive displacements along *b*.

(26) Kelty, S. P.; Lieber, C. M. *Phys. Rev. B* **1989**, *40*, 5856.
(27) Tarascon, J. M.; Miceli, P. F.; Barbaux, P.; Hwang, D. M.; Hull, G. W.; Giroud, M.; Greene, L. H.; LePage, V.; McKinnon, W. R.; Tselepis, E.; Pleizier, G.; Eibschutz, M.; Neumann, D. A.; Rhyne, J. J. *Phys. Rev. B* **1989**, *39*, 11587.

forward to determine the modulated atomic positions by examining cross sections along the *a* and *b* axes (Figure 3B,C). The atomic rows along the *a* direction show almost no lateral displacements; however, significant lateral displacements, 0.6 ± 0.3 Å, are observed along *b*. These displacements reflect the compression and expansion of the BiO layer atomic structure. Similar features have also been reported recently for the related system $Bi_2Sr_2CaCu_2O_y$.[11]

In contrast to the above $Bi_{2.2}Sr_{1.8}CuO_y$ data, images obtained on $Bi_{2.2}Sr_{1.8}Cu_{0.9}Fe_{0.1}O_y$ single crystals exhibit significant structural disorder (Figure 4). The average in-plane period of the BiO layer atomic structure, 3.8 ± 0.3 Å, is unchanged compared to that of the undoped material. The atomic structure does show random variations in the out-of-plane (*z*) corrugation. This disorder may be due to either electronic or structural effects but nevertheless can be associated with the substitution of Fe for Cu in these crystals. In addition, the superstructure detected in images of $Bi_{2.2}Sr_{1.8}Cu_{0.9}Fe_{0.1}O_y$ is not well-ordered, although on average it is still one-dimensional. The one-dimensional character of the superstructure is clearly apparent in two-dimensional Fourier transform (2DFT) power spectrum of this image (Figure 4B). The average modulation periods calculated directly from the image, 22.8 ± 1.0 Å, or using the 2DFT, 23 Å, are essentially the same. This average period is shorter than that observed in the pure material and is incommensurate with the underlying lattice. The average result determined from the 2DFT is also in agreement with electron diffraction measurements made on the Fe-doped samples (Figure 4C). The superlattice peaks observed in the diffraction patterns of the Fe-doped crystals are, however, significantly weaker than those observed in diffraction patterns for the pure materials.

Discussion

The structural modulation of the Bi-based superconductors has been the focus of numerous diffraction-based investigations.[3-8] Several factors have been proposed to explain the structure modulation, including (1) partial substitution of Sr for Bi in the BiO layers, (2) insertion of extra oxygen in the BiO layers, and (3) lattice mismatch between the CuO and BiO layers.[3-8,27-31] It is expected that substitution of Sr^{2+} (r = 1.32 Å) for Bi^{3+} (r = 1.17 Å) or incorporation of extra oxygen into the BiO layer would cause disorder in the atomic lattice. We have not, however, observed significant disorder in our images of the BiO surface of annealed $Bi_{2.2}Sr_{1.8}CuO_y$ crystals. Since Sr^{2+} or oxygen substitution would be expected to create disorder in the atomic lattice, these data indicate that substitution of Sr^{2+} for Bi^{3+} or the insertion of extra oxygen in the BiO layer may not cause the one-dimensional modulation. Data reported in other studies also support this suggestion. First, we have shown previously that oxygen removal from $Bi_2Sr_2CaCu_2O_y$ has little effect on the period of the superstructure.[14] In addition, a very recent high-temperature X-ray diffraction study of $Bi_2Sr_2CuO_x$ has also shown that the superstructure period does not change with oxygen content.[32] We thus believe that the dominant factor causing the modulation in the bismuth-based superconductors is the mismatch between CuO and BiO lattices. Substitution in the BiO layer (e.g. metals or oxygen) may, however, still perturb this structural modulation.

The importance of the interaction between the CuO and BiO layers in determining the superstructure is clearly seen in our data for the Fe-substituted materials. The images of $Bi_{2.2}Sr_{1.8}Cu_{0.9}Fe_{0.1}O_y$ (e.g., Figure 4A) exhibit significant disorder in the BiO layer superstructure which can be associated with the incorporation of iron into the solid. Since our analyses show that

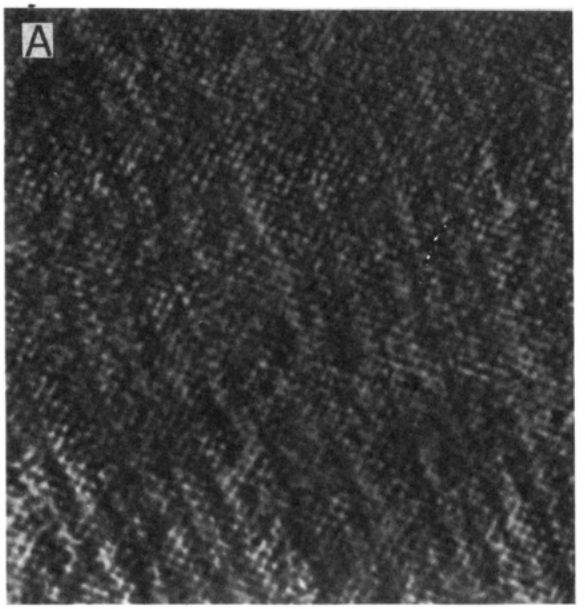

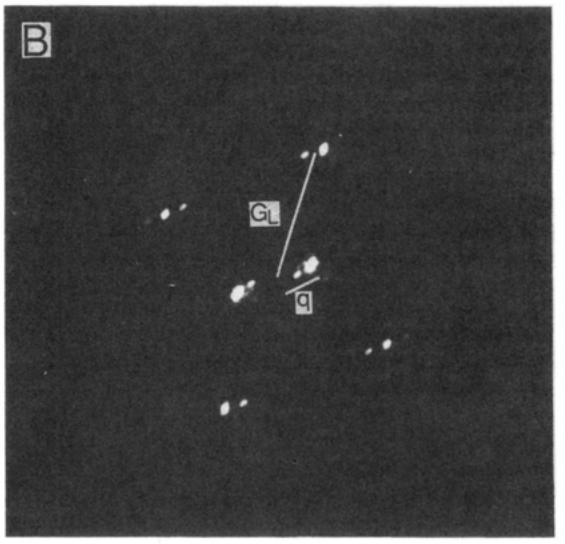

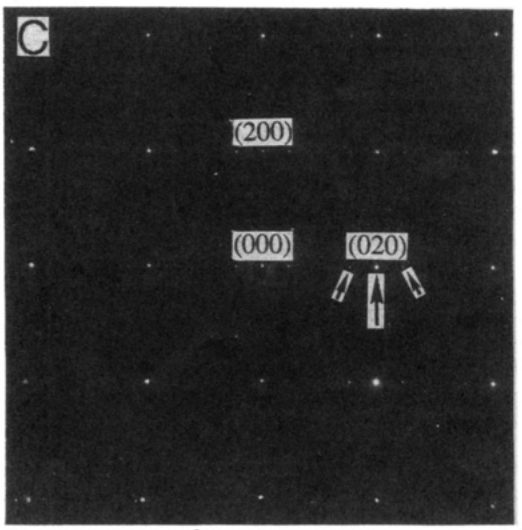

Figure 4. (A) 200 × 200 Å² STM image of $Bi_{2.2}Sr_{1.8}Cu_{0.9}Fe_{0.1}O_y$ recorded with a bias voltage of 61 mV and a tunneling current of 0.61 nA. (B) 2DFT power spectra corresponding to the image in (A). The atomic lattice and superstructure vectors are marked as $\mathbf{G}_L$ and $\mathbf{q}$, respectively. (C) [001] electron diffraction pattern acquired on a $Bi_{2.2}Sr_{1.8}Cu_{0.9}Fe_{0.1}O_y$ sample. The large arrow highlights the (020) diffraction peak (along b^*), and the small arrows mark superlattice reflections.

(28) Hiroi, Z.; Ikeda, Y.; Takano, M.; Bando, Y. *J. Mater. Res.* **1991**, *6*, 435.
(29) Horickhi, S.; Maeda, H.; Tanaka, Y.; Matsui, Y. *Jpn. J. Appl. Phys.* **1988**, *27*, L1172.
(30) Cheetham, A. K.; Chippindale, A. M.; Hibble, J. *Nature* **1988**, *21*, 333.
(31) Torardi, C. C.; Parise, J. B.; Subramanian, M. A.; Gopalakrishnan, J.; Sleight, A. W. *Physica C* **1989**, *157*, 115.
(32) Shen, Y.; Richards, D. R.; Hinks, D. G.; Mitchell, A. W. *Appl. Phys. Lett.* **1991**, *59*, 1559.

Fe substitutes primarily in the CuO layers, it is apparent that the interaction between the CuO and BiO layers must determine in part the superstructure. We suggest that the Cu apical oxygen which directly links the CuO and BiO layers (Figure 1) probably drives the disorder in the superstructure as a consequence of the difference in the Fe–O–Bi versus Cu–O–Bi bonding. The significance of the CuO and BiO lattice mismatch has also been discussed in previous diffraction investigations where it was suggested that the superstructure could be eliminated by substitution of the larger Pb^{2+} (r = 1.33 Å) cation for Bi^{3+} (r = 1.17 Å) in the BiO layer. In these studies no modulation was detected in diffraction data obtained on Pb-substituted $Bi_2Sr_2CuO_y$ and $BiPbSr_2MO_y$ (M = Mn, Fe, Co) materials.[33-35] Comparison of the STM and electron diffraction data for the Fe-doped system indicates that this conclusion may not be correct. We find that the superlattice peaks do become weaker with Fe substitution (as with Pb doping); however, the STM data demonstrate that this is due to increased disorder in the superlattice which reduces and ultimately eliminates the long-range coherence needed to observe diffraction.[36] STM can thus provide unique insight into the microstructure of these materials.

Lastly, we consider further the atomic structure of the BiO layer of $Bi_{2.2}Sr_{1.8}CuO_y$, $Bi_{2.2}Sr_{1.8}Cu_{0.9}Fe_{0.1}O_y$, and $Bi_2Sr_2CaCu_2O_8$. In all three materials the average lattice constant observed in the STM images, 3.8 Å, could correspond to the Bi–Bi or O–O distance. The similarity in the atomic structures suggests that the surface electronic states near the Fermi level, which are imaged by the STM, are similar for these three compounds. In contrast, recent photoemission spectroscopy (PES) data indicate that the π bands of the Bi–O layer do not cross the Fermi level (i.e., they are unoccupied) in $Bi_2Sr_2CuO_y$ but are partially filled in $Bi_2Sr_2CaCu_2O_y$.[25] Since it is possible that different crystal preparations may also contribute to the electronic character of the BiO layer, we cannot make a certain conclusion from the PES data at this point.[10,12,16] It will be important in the future to investigate by STM compositionally similar crystals that have electronically distinct BiO layers (these could be prepared using different annealing conditions) to address this point. There are, however, significant differences in the BiO layer atomic structure imaged in the pure and Fe-substituted materials. These differences indicate that either the surface BiO layer structure and/or electronic states are locally perturbed by the Fe in the underlying Cu(Fe)O layer or that the STM detects directly electronic states in the Cu(Fe)O layer. At present, we cannot unambiguously distinguish between these possibilities, although studies of the distance dependence of tunneling may resolve this question.[15,37]

Conclusions

In summary, STM has been used to characterize the surface structure of cleaved single crystals of $Bi_{2.2}Sr_{1.8}CuO_y$ and $Bi_{2.2}Sr_{1.8}Cu_{0.9}Fe_{0.1}O_y$ with atomic resolution for the first time. High-quality atomic resolution images of the BiO layer of $Bi_{2.2}Sr_{1.8}CuO_y$ show an incommensurate superstructure with a period of 25.1 ± 0.3 Å and an average atomic lattice spacing of 3.8 ± 0.2 Å. The atomic structure in these images is ordered and shows no evidence for local distortions due to Sr^{2+} substitution and/or extra oxygen in the BiO layer. The substitution of Cu with Fe causes distortions in the surface atomic structure and superstructure. Analyses of real-space images, 2DFT power spectra, and electron diffraction data show that the superstructure retains on average its one-dimensional character. The real-space STM data provide, however, detailed insight into the changes in the microstructure caused by Fe doping that cannot be detected by diffraction-based techniques. These data indicate that a mismatch between the BiO and CuO lattices is probably the dominant factor causing the one-dimensional modulation, although other effects may perturb this structure.

Acknowledgment. C.M.L. acknowledges support of this work by the National Science, David and Lucile Packard, Alfred P. Sloan, and Camille and Henry Dreyfus Foundations.

(33) Manivannan, V.; Gopalakrishnan, J.; Rao, C. N. R. *Phys. Rev. B* **1991**, *43*, 8686.
(34) Tarascon, J. M.; Page, Y. Le; McKinnon, W. R.; Ramesh, R.; Eibschutz, M.; Tselepis, E.; Wang, E.; Hull, G. W. *Physica C* **1990**, *167*, 20.
(35) Fukushima, N.; Niu, H.; Nakamura, S.; Takeno, S.; Hayashi, M.; Ando, K. *Physica C* **1989**, *159*, 777.
(36) STM studies of Pb-substituted $Bi_2Sr_2CuO_y$ show that a superstructure is present in these materials, although it exhibits significant disorder. The modulation is not detected by diffraction measurements since it lacks long-range coherence: Liu, J.; Lieber, C. M. Unpublished results.
(37) Zhang, Z.; Lieber, C. M. *J. Phys. Chem.* **1992**, *96*, 2030.

Collection Optics of TiO_2 Photocatalyst on Hollow Glass Microbeads Floating on Oil Slicks

I. Rosenberg,* J. R. Brock,* and A. Heller*

Department of Chemical Engineering, University of Texas at Austin, Austin, Texas 78712
(Received: October 9, 1991; In Final Form: December 19, 1991)

We analyze the optics of sunlight collection in hollow glass microbead attached TiO_2 particles floating on oil slicks, photoassisting their dissolution. This technology uses glass microbeads that float on the oil slick. The microbeads are partially coated with a layer of 3.0–3.3-eV bandgap TiO_2, a known catalyst for the photoassisted oxidation of organics. The fraction of the UV solar irradiance (λ = 360 nm) directly and indirectly exciting the TiO_2 photocatalyst is calculated. It is shown that a glass microbead collects most of the sunlight, channeling it to the attached photocatalyst particles. Therefore, 30–40% coverage of the microbeads is optimal for photodissolving oil slicks. Here, the collection optics of the floating, coated microbeads is analyzed.

Introduction

Our proposed method developed for solar-assisted oxidation of oil slicks involves the use of the classical semiconducting photocatalyst titanium dioxide. Upon absorption of a photon, an electron–hole pair is generated in the TiO_2 microcrystal. The electron may react with surface-adsorbed oxygen, reducing it to hydrogen peroxide; the hole oxidizes adsorbed water to OH radicals and photons; the OH radicals oxidize in turn adsorbed organic compounds. Titanium dioxide is denser than either oil or seawater; the density of the anatase phase is 3.8, and that of

0022-3654/92/2096-3423$03.00/0